

Parthenolide induces ROS-dependent cell death in human gastric cancer cell

*Dandan Han^{1,B,D}, *Wenhao Zhu^{2,B,D}, Yang Chen^{1,B,E}, Huiru Wang^{1,A,C,E,F}

¹ Department of Transfusion, The First Affiliated Hospital of University of Science and Technology of China (USTC), Division of Life Sciences and Medicine, University of Science and Technology of China, Hefei, China

² Institute of Integrated Medicine, School of Basic Medicine, Qingdao University, China

A – research concept and design; B – collection and/or assembly of data; C – data analysis and interpretation; D – writing the article; E – critical revision of the article; F – final approval of the article

Advances in Clinical and Experimental Medicine, ISSN 1899–5276 (print), ISSN 2451–2680 (online)

Adv Clin Exp Med. 2024;33(11):1237–1245

Address for correspondence

Huiru Wang

E-mail: wanghuiru@ustc.edu.cn

Funding sources

This study was supported by the National Natural Science Foundation of China (grant No. 81903637), the Fundamental Research for the Central Universities (grant No. WK9110000027), the Natural Science Foundation of Anhui Province (grant No.1708085QH198), Youth Foundation of Anhui Province Cancer Hospital (grant No. 2020YJQN018), and the Anhui Provincial Postdoctoral Science Foundation. The RNA-seq was supported by the Genergy Biotechnology of Shanghai.

Conflict of interest

None declared

*Dandan Han and Wenhao Zhu contributed equally to this work.

Received on March 14, 2023

Reviewed on June 4, 2023

Accepted on November 13, 2023

Published online on January 10, 2024

Abstract

Background. Parthenolide (PN), a key active ingredient of feverfew, has been used to treat gastrointestinal disorders. However, the mechanism of the cytotoxic effect exerted by PN on tumor cells has not been elucidated.

Objectives. To study the cytotoxic effect of PN on human gastric cancer cells, the specific death mode, and gene expression changes induced by PN.

Materials and methods. In this study, MGC-803 cells were used to study PN-induced cytotoxicity as a gastric cancer cell line. Assays of cell proliferation, cell cycle distribution, apoptosis, and reactive oxygen species (ROS) were performed using a Cell Counting Kit-8 (CCK-8) assay and a flow cytometer. MGC-803 cells treated with and without PN were separately subjected to high-throughput RNA sequencing. Western blotting was used to investigate the expression of some important proteins.

Results. Parthenolide exposure elicited cell proliferation inhibition in a dose- and time-dependent manner. Parthenolide induced cell cycle arrest at the G1 and S stages. Parthenolide-induced caspase-dependent apoptosis and necroptosis were caused by the activation of RIP, RIP3 and MLKL. MGC-803 cells showed a response to ROS and oxidative stress after PN treatment. Moreover, ROS and cytotoxicity induced by PN were significantly attenuated by a ROS scavenger catalase.

Conclusions. Parthenolide-induced gastric cancer cell death is a complex ROS-dependent process different from ordinary apoptosis and necrosis, suggesting that PN is a potential treatment option for gastric cancer.

Key words: cytotoxicity, reactive oxygen species, apoptosis, gastric cancer, parthenolide

Cite as

Dandan Han D, Zhu W, Chen Y, Wang H. Parthenolide induces ROS-dependent cell death in human gastric cancer cell..

Adv Clin Exp Med. 2024;33(11):1237–1245.

doi:10.17219/acem/175152

DOI

10.17219/acem/175152

Copyright

Copyright by Author(s)

This is an article distributed under the terms of the Creative Commons Attribution 3.0 Unported (CC BY 3.0) (<https://creativecommons.org/licenses/by/3.0/>)

Background

Parthenolide (PN), a sesquiterpene lactone derived from feverfew, which is the traditional herbal medicine, has been found to exert multiple pharmacological effects such as anti-microbial, anti-inflammatory and anti-cancer effects.^{1–3} These biological properties of PN may be attributed to its α -methylene- γ -lactone moiety.⁴ At present, strong inhibition of nuclear factor NF- κ B (nuclear factor kappa-light-chain-enhancer of activated B cells) along the NF- κ B signaling pathway in multiple steps makes PN the inhibitor of NF- κ B.⁵ However, the underlying mechanisms in the cytotoxic effect of PN on tumor cells are still not fully elucidated.

Several recent studies indicate that apoptosis and autophagy are involved in PN-induced cell death in tumor cells. However, it is unclear whether other cell death forms are involved in PN-induced cell death.^{6–8} To differ from the old and inappropriate definition of cell death formulated from the morphological perspective, regulated cell death (RCD) is newly classified into multiple forms including apoptosis, pathanatos, necroptosis, pyroptosis, and ferroptosis.⁹

Reactive oxygen species (ROS), a heterogeneous group of oxygen-containing radical species, participates in a wide range of biochemical processes in tumor cells.¹⁰ The function of ROS is decided by its level. For instance, persistently high levels of ROS could be beneficial to tumorigenesis and metastasis.¹¹ Reactive oxygen species participate in the initiation, progression and metastasis of gastric cancer cells. However, further exposure to higher ROS induces serious oxidative stress which facilitates cell death.¹² Thus, induction of oxidative damage may be a therapeutic approach for gastric cancer.¹³ It has been reported that PN causes oxidative stress by inducing ROS generation; however, ROS and PN-induced cell death are not well understood.^{14,15}

Objectives

To study the cytotoxic effect of PN on human gastric cancer cells, the specific death mode and gene expression changes induced by PN.

Materials and methods

Reagents

Parthenolide, Z-VAD-fmk, AG14361, and Nec-1 were all supplied by Selleck (Houston, USA). Catalase and dimethyl sulfoxide (DMSO) were supplied by Beyotime Biotechnology (Shanghai, China).

Cell culture and treatment

The MGC-803 cell line was purchased from the National Infrastructure of Cell Line Resource (Beijing, China) and

cultured at 37°C, 5% CO₂ in Dulbecco's modified Eagle's medium (DMEM)/high glucose supplemented with 10% fetal bovine serum (FBS; Gibco, Waltham, USA). We incubated cells in 96-well plates (1×10⁴ cells/well) and 6-cm dishes (6×10⁵ cells/dish) for 24 h. Then, MGC-803 was treated with PN at indicated concentrations for the indicated time with or without 1 h pretreatment with Z-VAD-fmk, AG14361, Nec-1, and catalase. We followed the methods of the previous study.¹⁶

Cell cycle assay

Cell cycles were identified using a cell cycle assay kit (Beyotime Biotechnology). MGC-803 cells were harvested after treatment and washed with phosphate-buffered saline (PBS), then fixed with 70% ethanol overnight at 4°C. For staining, cells were incubated at room temperature with 40 mg/mL propidium iodide (PI), followed by 30 min at room temperature in the dark, and then analyzed using a flow cytometer (BD Accuri C6; BD Biosciences, Franklin Lakes, USA).

Colony formation assay

MGC-803 cells were plated into the 6-well plate (2×10³ cells/well) with treatment or control and grown for 2 weeks at 37°C, 5% CO₂. The cell colonies were stained with crystal violet and the colony numbers were recorded.

ROS assay

An ROS assay kit was used to measure the intracellular ROS levels (Beyotime Biotechnology). After treatment, cells were harvested and washed with PBS, and then incubated with dichlorodihydrofluorescein diacetate (DCFH-DA) (50 μ M) containing PBS solution for 30 min at 37°C in the dark and analyzed with a flow cytometer.

Cell apoptosis assay

The annexin-V/PI staining kit (EpiZyme Biotech, Cambridge, USA) was used to identify cell apoptosis. Cells were harvested, washed with PBS, stained with 10 μ M annexin-V and 5 μ M PI in the dark for 15 min at 37°C, and then analyzed with a flow cytometer.

RNA sequencing (RNA-seq)

MGC-803 cells treated with DMSO or PN (40 μ M) for 24 h were collected and the RNA samples were isolated with Trizol according to the manufacturer's instructions. After the cDNA was synthesized, the library was sequenced using Illumina NovaSeq6000 platform (Illumina, San Diego, USA). The abundance of genes was estimated using featureCounts program (<https://subread.sourceforge.net>). Differentially expressed genes between

DMSO-treated and DMSO-treated MGC-823 cells were identified using DEseq2. Original RNA-seq data have been deposited in the National Center for Biotechnology Information Gene Expression Omnibus repository (GSE217526). Differentially expressed genes (DEGs) were defined as genes with a p-value >0.05 and absolute fold change >2 . Gene Ontology (GO) functional enrichment analysis was used to identify significantly enriched GO terms in DEGs.

Western blot analysis

Radioimmunoprecipitation assay (RIPA) lysis buffer was used for total protein extraction and a BCA assay was applied to identify protein concentrations. Samples (40 μ g each) were separated using 10–15% sodium dodecyl-sulfate polyacrylamide gel electrophoresis (SDS-PAGE) and transferred to polyvinylidene difluoride (PVDF) membranes. The membranes were incubated with specific primary antibodies after blocking. The antibodies against p53, cyclin D1, cyclin E1, p21^{WAF1/CIP1}, p27^{KIP1}, caspase-3, caspase-9, caspase-8, c-FLIP, poly(ADP-ribose)polymerase 1 (PARP-1), BCL2, BAX, BAK, p-receptor-interacting serine/threonine kinase (pRIP), RIP, p-RIP3, RIP3, and p-mixed lineage kinase domain-like pseudo kinase (MLKL) were obtained from Cell Signaling Technology (CST; Danvers,

USA; 1:1,000 dilution), and β -actin was obtained from ABClonal Biotech (1:5,000 dilution; Wuhan, China). The protein bands were visualized using chemiluminescent detection.

Statistical analyses

GraphPad Prism 7 software (GraphPad Software, San Diego, USA) and IBM SPSS v. 22 (IBM Corp., Armonk, USA) was used to perform the statistical analysis. Data are shown as data points with the median and analyzed using 2-sided Wilcoxon rank-sum test (2 groups) or Kruskal–Wallis tests and the post hoc Dunn's test (more than 2 groups). A p-value of <0.05 and $0.05 < p < 0.1$ are considered statistically significant and marginally statistically significant, respectively. The original data analysis was shown in the Supplementary material.

Results

The growth of human gastric cancer cell MGC-803 was inhibited after PN treatment

To explore the effect of PN on tumor cell growth, CCK-8 was used to detect cell viability. As shown in Fig. 1A, PN exposure inhibited cell viability in a dose- and time-dependent

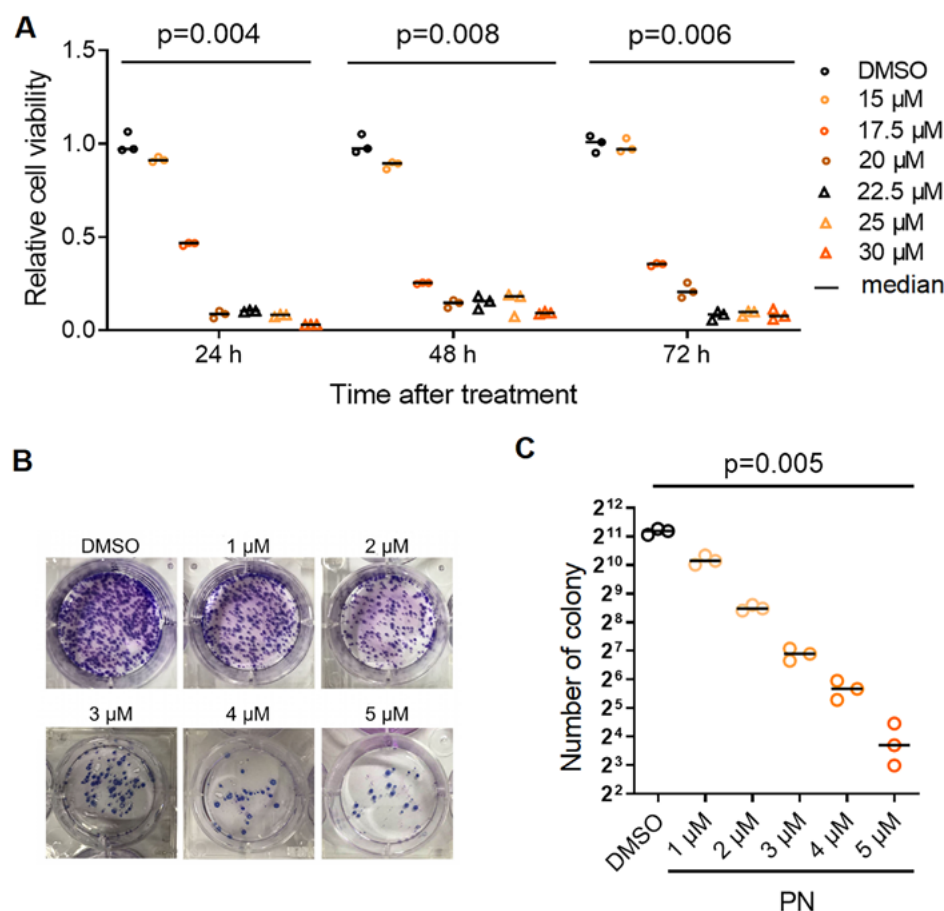


Fig. 1. The growth of human gastric cancer cell MGC-803 was inhibited after parthenolide (PN) treatment. **A.** MGC-803 cells were treated with dimethyl sulfoxide (DMSO) and PN (15, 17.5, 20, 22.5, 25 μ M) for 24 h, 48 h and 72 h, and then the cell viability was measured using Cell Counting Kit-8 (CCK-8) assay. Three culture plates were used in total and in each plate 3 culture replicates per condition were set up. After 24 h of culture, CCK-8 was added to the 1st culture plate and proliferation was evaluated based on the optical density (OD) values. After incubation for 48 h and 72 h, the 2nd and 3rd culture plates were removed, and proliferation was detected in a similar manner; **B.** C. MGC-803 cells were treated with DMSO and PN (1, 2, 3, 4, 5 μ M) for 2 weeks and then colony numbers were recorded. Each experimental group was equipped with 3 repeated wells. Each dot or triangle represents each well. Representative images of cell clonal staining (**B**) and statistical analysis of colony numbers (**C**) were shown. **A.** Kruskal–Wallis test, 24 h: $p=0.004$, $H=18.327$, $df=6$; 48 h: $p=0.008$, $H=18.327$, $df=6$; 72 h: $p=0.006$, $H=18.327$, $df=6$. **C.** Kruskal–Wallis test, $p=0.005$, $H=18$, $df=5$

manners (Kruskal–Wallis test, 24 h: $p = 0.004$, $H = 18.327$, $df = 6$; 48 h: $p = 0.008$, $H = 18.327$, $df = 6$; 72 h: $p = 0.006$, $H = 18.327$, $df = 6$). Compared with the control, when PN was used at a concentration of 20 μM , the growth of half of the cells was inhibited (Supplementary Table 1). Moreover, the results of the colony formation assay showed that the growth of MGC-803 cells exposed to PN for 2 weeks was inhibited in a dose-dependent manner (Fig. 1B,C, Supplementary Table 2, Kruskal–Wallis test, $p = 0.005$, $H = 18$, $df = 5$).

MGC-803 showed G1 and S phase cell cycle arrest after PN treatment

Since the cell cycle plays an important role in the development of cancer, we use PI staining to identify the effects of PN on the cell cycle of MGC-803 cells. As shown in Fig. 2A,B, the cell cycle of MGC-803 cells exposed to PN showed a strong tendency to be selectively arrested at the G₁ and S phases (2-sided Wilcoxon rank-sum test, $p = 0.081$, $T = 6$). Furthermore, PN exposure induced the increase of protein levels of p53, p21^{WAF1/CIP1} and p27^{KIP1}, while the protein levels of cyclin D1 and cyclin E1 were decreased (Fig. 2C), indicating that PN may induce G₁ and S cell cycle arrest.

The expression of apoptosis and necrosis related proteins in MGC-803 cells increased after PN treatment

We used annexin-V/PI staining to identify whether PN induced apoptosis in MGC-803 cells. Parthenolide exposure elicited a marginal statistically significant increase in the apoptotic cell population (Fig. 3A, 2-sided Wilcoxon rank-sum test, $p = 0.081$, $T = 6$), indicating that apoptosis occurred after PN treatment. Furthermore, as shown in Fig. 3B, PN exposure elicited an increase in cleaved caspase-3 (19 kDa and 17 kDa), cleaved caspase-9 (37 kDa, 35 kDa), cleaved caspase-8 (43 kDa), and cleaved PARP1 (87 kDa), indicating that PN exposure activated caspase-3, caspase-9, caspase-8, and PARP1 in MGC-803 cells. Furthermore, both protein levels of c-FLIP_L and c-FLIP_S, 2 isoforms of c-FLIP (cellular FLICE-like inhibitory proteins) endowed with inhibitory activity in caspase-8 activation, appeared to decrease over time after PN treatment, indicating that extrinsic apoptosis propagated by caspase-8 was involved in PN-induced cell death in MGC-803 cells. On the other hand, after PN exposure, both the protein levels of BAX and BAK which were implicated in intrinsic apoptosis appeared to increase over time, while BCL2 protein levels appeared unchanged, indicating that intrinsic apoptosis was also involved in PN-induced cell death in MGC-803 cells (Fig. 3C).

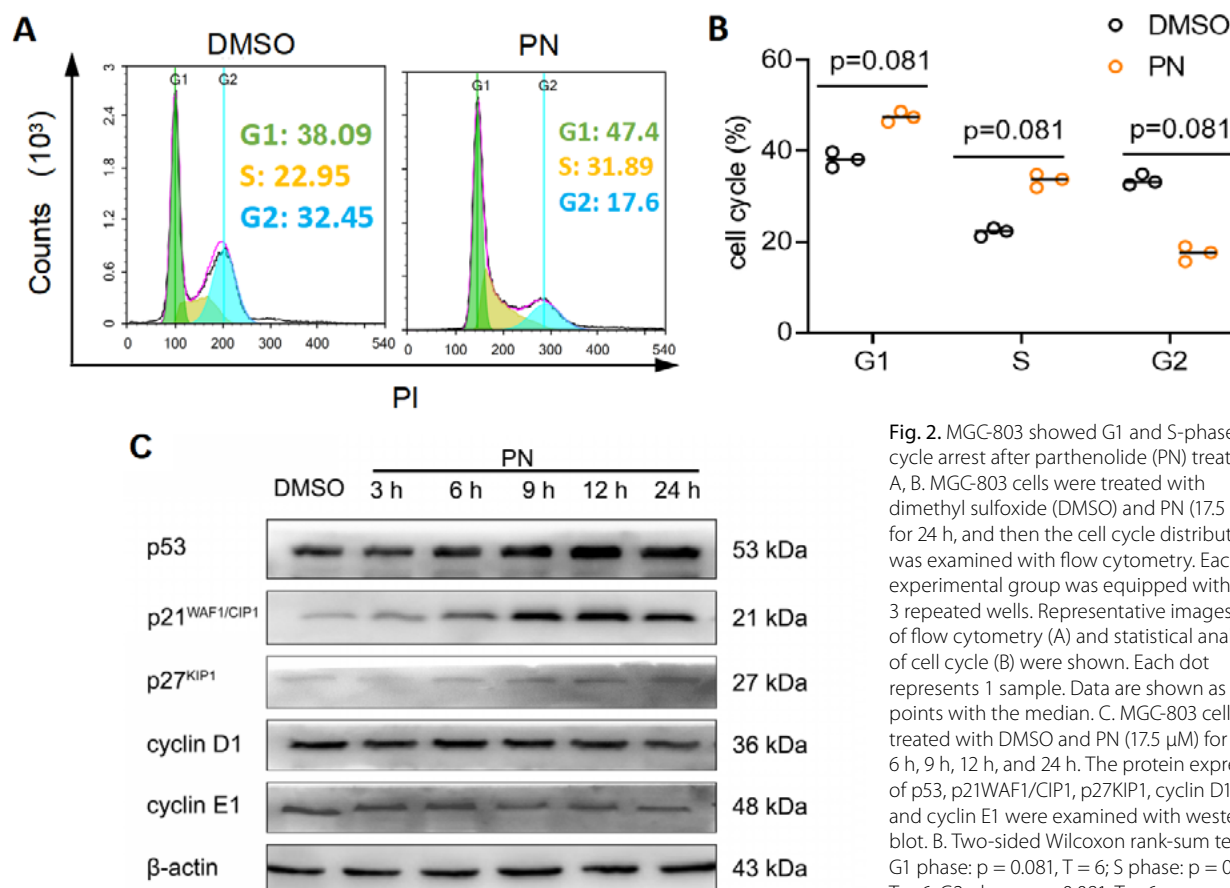


Fig. 2. MGC-803 showed G1 and S-phase cell cycle arrest after parthenolide (PN) treatment. A, B. MGC-803 cells were treated with dimethyl sulfoxide (DMSO) and PN (17.5 μM) for 24 h, and then the cell cycle distribution was examined with flow cytometry. Each experimental group was equipped with 3 repeated wells. Representative images of flow cytometry (A) and statistical analysis of cell cycle (B) were shown. Each dot represents 1 sample. Data are shown as data points with the median. C. MGC-803 cells were treated with DMSO and PN (17.5 μM) for 3 h, 6 h, 9 h, 12 h, and 24 h. The protein expression of p53, p21^{WAF1/CIP1}, p27^{KIP1}, cyclin D1, and cyclin E1 were examined with western blot. B. Two-sided Wilcoxon rank-sum test, G1 phase: $p = 0.081$, $T = 6$; S phase: $p = 0.081$, $T = 6$; G2 phase: $p = 0.081$, $T = 6$.

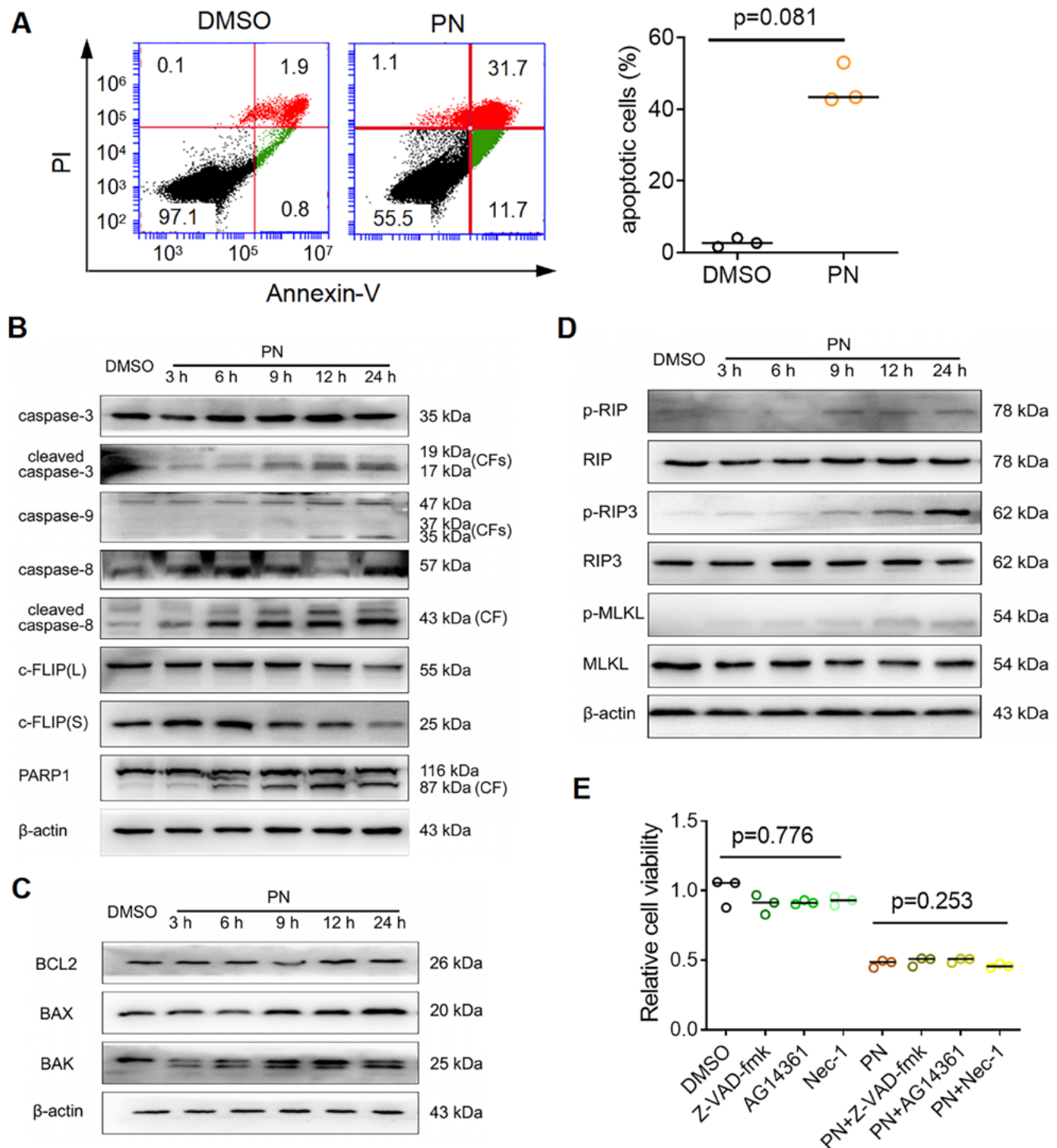


Fig. 3. The expression of apoptosis- and necrosis-related proteins in MGC-803 cells increased after parthenolide (PN) treatment. **A.** MGC-803 cells were treated with DMSO and PN (17.5 μ M) for 3 h, 6 h, 9 h, 12 h, and 24 h. The cell apoptotic population was examined with flow cytometry after annexin-V/PI staining. Representative images of flow cytometry (left panel) and statistical analysis of apoptosis (right panel) were shown. Each experimental group was equipped with 3 repeated wells. Each dot represents 1 sample; **B.** The protein levels of caspase-3, caspase-8, caspase-9, PARP-1, and c-FLIP were examined using western blot after treatment; **C.** The protein levels of BCL2, BAX and BAK were examined with western blot after treatment; **D.** The protein levels of p-RIP, RIP, p-RIP3, RIP3, p-MLKL, and MLKL were examined with western blot; **E.** MGC-803 cells were treated with PN (17.5 μ M) with or without 1 h pretreatment with Z-VAD-fmk (100 μ M), AG14361 (50 μ M) or Nec-1 (50 μ M). Cell viability was measured using Cell Counting Kit-8 (CCK-8) assay after culture for 24 h. Data are shown as data points with the median (A, E). **A.** Two-sided Wilcoxon rank-sum test, $p = 0.081$, $T = 6$, Kruskal–Wallis test, $p = 0.776$, $H = 1.333$, $df = 3$; $p = 0.253$, $H = 4$, $df = 3$

We also examined whether necroptosis was induced by PN exposure in human gastric cancer cells. Necroptosis is an RCD type that involves the activation of RIP, RIP3 and MLKL. As shown in Fig. 3D, PN exposure elicited

an increase in RIP phosphorylation (Ser166), RIP3 phosphorylation (Ser227) and MLKL phosphorylation (Ser358), indicating that PN may induce necroptosis in human gastric cancer cells. Next, we used Z-VAD-fmk (pan-caspase

inhibitor), AG14361 (PARP1 inhibitor) and Nec-1 (RIP1 inhibitor) to detect whether apoptosis and necroptosis induced by PN can be inhibited. As shown in Fig. 3E, pretreatment of all 3 inhibitors in MGC-803 cells could not mitigate PN-induced cytotoxicity, indicating that PN-induced cytotoxicity was a complicated process (Kruskal–Wallis test, $p = 0.776$, $H = 1.333$, $df = 3$; $p = 0.253$, $H = 4$, $df = 3$).

High-throughput sequencing showed that the oxidative stress response was enhanced after PN treatment

To comprehensively analyze the changes in cancer cells caused by PN treatment, the transcriptomes of PN-treated MGC-803 cells with control (DMSO-treated) were profiled using RNA-Seq. Heat maps were drawn based on FPKM

(fragments per kilobase million) values for hundreds of DEGs identified between the groups (Fig. 4A). Collectively, the up-regulation of expression of 832 unique transcripts and downregulation of 1,278 transcripts was evident in the transcriptional profiles of PN-treated MGC-803 cells compared to the control (Fig. 4B). Next, we found that “response to oxidative stress” and “response to reactive oxygen species” were enriched at the top of GO Biological Process terms enrichment (Fig. 4C). These results indicated that response to ROS may be involved in cytotoxicity induced by PN.

Cytotoxicity induced by PN was attenuated by catalase in MGC-803

Since the sequencing results suggested that ROS are closely related to cell death induced by PN, we also used

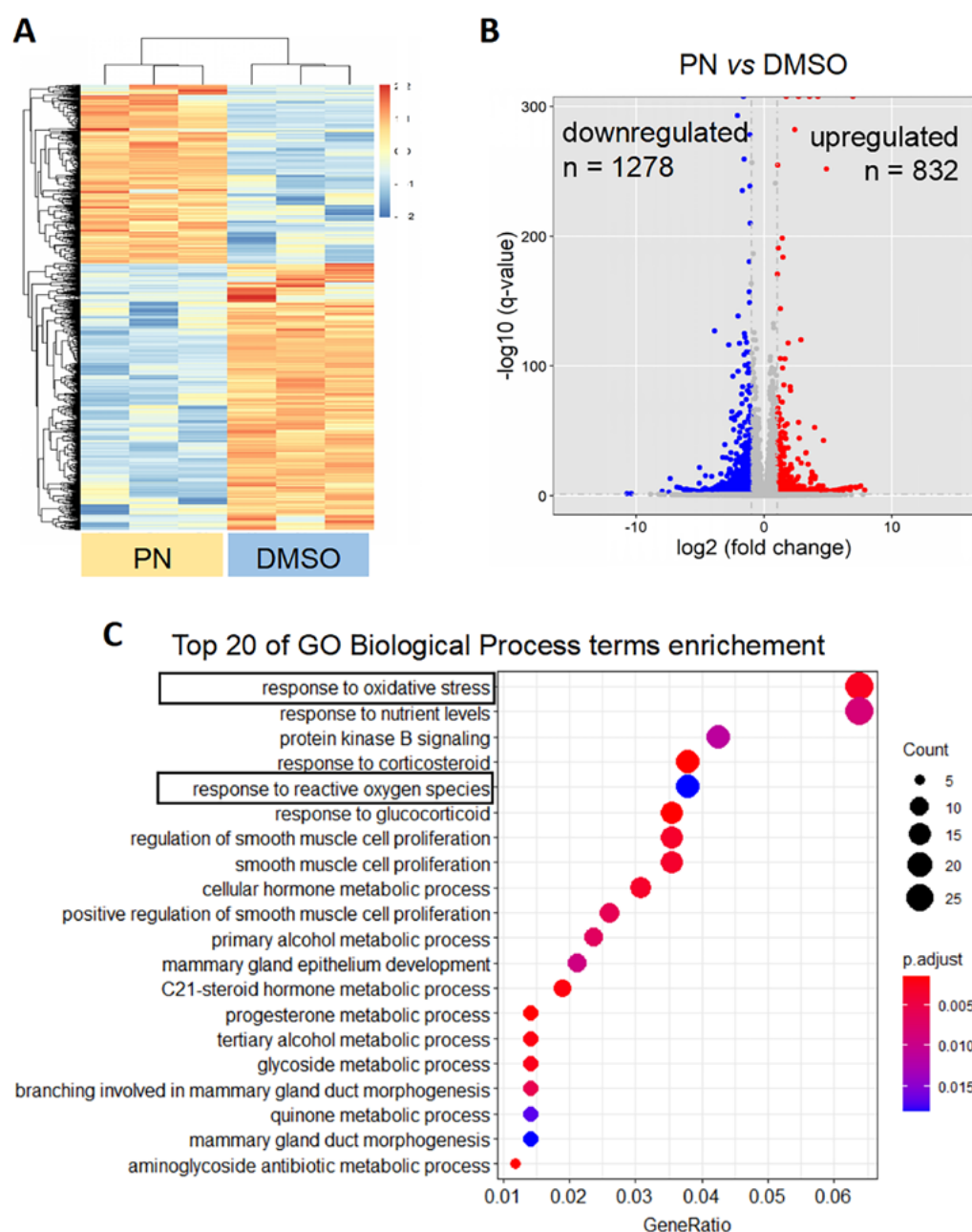


Fig. 4. High-throughput sequencing showed that the oxidative stress response was enhanced after parthenolide (PN) in MGC-803. A. The differentially expressed genes (DEGs) (fold change >2 and p -value <0.05) of MGC-803 cells treated with dimethyl sulfoxide (DMSO) compared with their counterparts treated with PN for 24 h were selected for heat map analysis. Each column represents 1 sample ($n = 3$ per group); B. DEGs, including upregulated genes ($n = 832$) and downregulated genes ($n = 1,278$), were illustrated using a volcano plot: PN treatment compared to DMSO treatment; C. Top 20 biological processes obtained with GO enrichment of DEGs

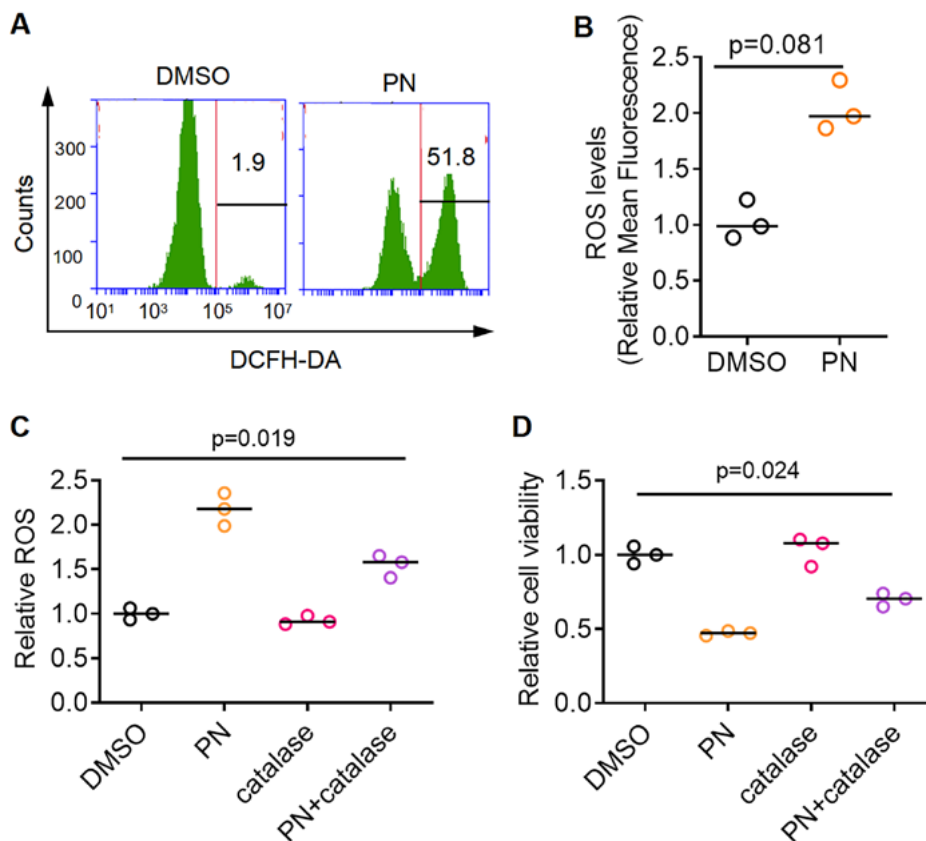


Fig. 5. Cytotoxicity induced by parthenolide (PN) was attenuated using catalase in MGC-803. **A.** The intracellular reactive oxygen species (ROS) levels of MGC-803 cells treated with dimethyl sulfoxide (DMSO) and PN (17.5 μ M) for 24 h were measured using flow cytometry; **B.** Quantification of relative mean fluorescence of ROS level; **C, D.** The relative intracellular ROS and viability of MGC-803 cells treated with DMSO, PN (17.5 μ M), catalase (2,000 U/mL), or co-treatment with PN and catalase was measured with flow cytometry and Cell Counting Kit-8 (CCK-8) assay. Each experimental group was equipped with 3 repeated wells. Data are shown as data points with the median. **B.** Two-sided Wilcoxon rank-sum test, $p = 0.081$, $T = 6$. **C.** Kruskal–Wallis test, $p = 0.019$, $H = 9.974$, $df = 3$. **D.** Kruskal–Wallis test, $p = 0.024$, $H = 9.462$, $df = 3$

DCFH-DA staining to determine ROS levels. As shown in Fig. 5A,B, PN exposure elicited a marginal statistically significant increase in ROS levels in MGC-803 cells (2-sided Wilcoxon rank-sum test, $p = 0.081$, $T = 6$). Furthermore, the ROS quencher catalase was used to identify the role of ROS in PN-induced cytotoxicity, and the results showed that pretreatment of catalase significantly attenuated the increase of ROS levels (Fig. 5C, Supplementary Table 3, Kruskal–Wallis test: $p = 0.019$, $H = 9.974$, $df = 3$; post hoc Dunn's test, DMSO compared to PN + catalase: $p = 0.258$) and cell death (Fig. 5D, Supplementary Table 4, Kruskal–Wallis test: $p = 0.024$, $H = 9.462$, $df = 3$; post hoc Dunn's test, DMSO compared to PN + catalase: $p = 0.174$) induced by PN, indicating that ROS may be critical in PN-induced cytotoxicity.

Discussion

Parthenolide, a sesquiterpene lactone derived from feverfew, has shown cytotoxic activity in multiple human cancer cells, such as glioblastoma cells,¹⁷ breast cancer cells,¹⁸ renal cell carcinoma,¹⁹ and colorectal cancer.²⁰ There has not yet been a complete explanation of the mechanism behind PN-induced cell death. In this study, the biological effects of PN were investigated in human gastric cancer cells MGC-803.

In our study, PN inhibited cell growth in a dose- and time-dependent manner, demonstrating its cytotoxic

effect. In addition, we demonstrated that PN can induce tumor cell arrest in G1 and S phases, which is consistent with some other studies.^{21,22} There are various types of cyclins, cyclin-dependent kinases and other regulatory proteins that regulate cell cycle progression. Among them, p53 controls 3 cell cycle checkpoints. For G1 to S, cyclin D1 and cyclin E1 are the positive regulators, and p21^{WAF1/CIP1} and p27^{KIP1} are the negative regulators.²³ In this study, PN treatment upregulated the p53 protein levels in MGC-803 cells compared with those in DMSO-treated cells, indicating that PN may activate p53. In addition, PN exposure downregulated the protein levels of cyclin D1 and cyclin E1 in MGC-803 cells, indicating that PN may induce G1 phase arrest. Moreover, the present study also examined 2 negative regulators, p21^{WAF1/CIP1} and p27^{KIP1}, which restraint G1-S progression, and the results showed that PN exposure upregulated the protein levels of p21^{CIP1} and p27^{KIP1} in MGC-803 cells compared with those in DMSO-treated cells, confirming that PN induced G1 and S-phase arrest.

Cytotoxicity of PN involves several RCD types; among them, apoptosis serves a very essential part in PN-induced cell death in several cancer cells models.^{24,25} Likewise, our results show that PN exposure elicited a significant increase in the apoptotic cell population in MGC-803 cells. BCL2 and BAX mediate irreversible mitochondrial outer membrane permeabilization (MOMP), an essential step in mitochondrial-dependent intrinsic apoptosis.^{26,27} In the present study, both the protein levels of BAX and

BAK in MGC-803 cells treated with PN increased over time, while BCL2 protein levels appeared unchanged, suggesting that intrinsic apoptosis may be involved in PN-induced cell death. Extrinsic apoptosis was propagated by caspase-8 and precipitated by executioner caspases, mainly caspase-3. In the present study, PN exposure activated caspase-8 and downregulated the protein levels of caspase-8 inhibitors, c-FLIP, indicating that extrinsic apoptosis may be also involved in PN-induced cell death in MGC-803 cells.²⁸ Moreover, we also found that PN exposure elicited an increase of cleaved PARP1, indicating that PARP1 was activated. PARP1 activation can occur in response to DNA damage, leading to $\Delta\psi$ m dissipation and MOMP.²⁹

Necroptosis is a type of RCD that manifests a necrotic morphotype. Its main mechanism is the sequential activation of RIP, RIP3 and MLKL.^{30,31} Our results show that in MGC-803 cells, PN exposure elicited an increase of RIP, RIP3 and MLKL phosphorylation, indicating that RIP, RIP3 and MLKL may be activated by PN exposure to precipitate necroptosis.

A lot of evidence suggests that for the processes that are referred to as necessary steps for the execution of cell death, pharmacologic inhibition only changes its biochemical and morphological manifestations, but could not effectively prevent cell death.^{32–34} For example, although the inhibitors of caspase, PARP1 and RIP can significantly block the activation of caspases, PARP1 and RIP induced by pharmacologic interventions, cell death remain unchanged.³⁵ Likewise, our results show that Z-VAD-fmk, AG14361 or Nec-1 failed to protect MGC-803 cells from cell death.

In the whole process of RCD, the reverse of early-phase biochemical changes such as decreasing ATP levels and oxidative stress could restore cellular homeostasis.³² Our results show that in MGC-803 cells, PN exposure elicited a significant increase in ROS, while pretreatment of the ROS scavenger catalase significantly attenuated this effect. Moreover, pretreatment of catalase effectively inhibited the decrease of cell viability induced by PN exposure, indicating that PN-induced cytotoxicity is ROS-dependent.

Limitations

Due to the poor solubility of PN, more improvements in the dosage form are needed for its clinical application in the future. Similarly, the forms of drug dosage also limit experiments on animals.

Conclusions

Parthenolide-induced gastric cancer cell death is a complex ROS-dependent process different from ordinary apoptosis and necrosis, suggesting that PN is a potential treatment option for gastric cancer.

Supplementary data

The Supplementary materials are available at <https://doi.org/10.5281/zenodo.10066470>. The package includes the following files:

Supplementary Table 1. Post hoc Dunn's test for the effect of PN on the cell viability of MGC-803 cell.

Supplementary Table 2. Post hoc Dunn's test for the effect of PN on the cell colonies of MGC-803 cells.

Supplementary Table 3. Post hoc Dunn's test for the effect of PN and catalase on ROS Generation of MGC-803 cells.

Supplementary Table 4. Post hoc Dunn's test for the effect of PN and catalase on cell viability of MGC-803 cells.

Supplementary Table 5. Original data. Parthenolide induces ROS-dependent cell death in human gastric cancer cell analysis.

Supplementary Table 6. Gene sample count from MGC-803 cells treated with DMSO compared with counterparts treated with PN.


Data availability


The datasets generated and/or analyzed during the current study are available from the corresponding author on reasonable request.


Consent for publication


Not applicable.

ORCID iDs

Dandan Han  <https://orcid.org/0000-0003-0000-5541>

Wenhao Zhu  <https://orcid.org/0009-0008-0460-2283>

Yang Chen  <https://orcid.org/0000-0002-9449-3699>

Huiru Wang  <https://orcid.org/0000-0003-3026-6005>

References

1. Liu L, Liu N, Zhang H, Li D. Exploring and validating the metastasis mechanism of parthenolide interfering with cutaneous melanoma through ER stress-dependent apoptosis based on the network pharmacology. *Phytochem Anal.* 2023;34(7):745–754. doi:10.1002/pca.3193
2. Zhang Y, Feng W, Peng X, et al. Parthenolide alleviates peritoneal fibrosis by inhibiting inflammation via the NF- κ B/TGF- β /Smad signaling axis. *Lab Invest.* 2022;102(12):1346–1354. doi:10.1038/s41374-022-00834-3
3. Liu M, Xiao C, Sun M, Tan M, Hu L, Yu Q. Parthenolide inhibits STAT3 signaling by covalently targeting Janus kinases. *Molecules.* 2018; 23(6):1478. doi:10.3390/molecules23061478
4. Tyagi V, Alwaseem H, O'Dwyer KM, et al. Chemoenzymatic synthesis and antileukemic activity of novel C9- and C14-functionalized parthenolide analogs. *Bioorg Med Chem.* 2016;24(17):3876–3886. doi:10.1016/j.bmc.2016.06.028
5. Li Y, Xu H, Tan X, et al. Parthenolide inhibits proliferation of cells infected with Kaposi's sarcoma-associated herpesvirus by suppression of the NF- κ B signaling pathway. *Arch Virol.* 2023;168(2):39. doi:10.1007/s00705-022-05626-0
6. Yi J, Gong X, Yin XY, et al. Parthenolide and arsenic trioxide co-trigger autophagy-accompanied apoptosis in hepatocellular carcinoma cells. *Front Oncol.* 2022;12:988528. doi:10.3389/fonc.2022.988528
7. Cui M, Wang Z, Huang LT, Wang JH. Parthenolide leads to proteomic differences in thyroid cancer cells and promotes apoptosis. *BMC Complement Med Ther.* 2022;22(1):99. doi:10.1186/s12906-022-03579-0

8. Hu B, Zhen D, Bai M, et al. Ethanol extracts of *Rhaponticum uniflorum* (L.) DC flowers attenuate doxorubicin-induced cardiotoxicity via alleviating apoptosis and regulating mitochondrial dynamics in H9c2 cells. *J Ethnopharmacol.* 2022;288:114936. doi:10.1016/j.jep.2021.114936
9. Galluzzi L, Vitale I, Aaronson SA, et al. Molecular mechanisms of cell death: Recommendations of the Nomenclature Committee on Cell Death 2018. *Cell Death Differ.* 2018;25(3):486–541. doi:10.1038/s41418-017-0012-4
10. Dickinson BC, Chang CJ. Chemistry and biology of reactive oxygen species in signaling or stress responses. *Nat Chem Biol.* 2011;7(8):504–511. doi:10.1038/nchembio.607
11. Moloney JN, Cotter TG. ROS signalling in the biology of cancer. *Semin Cell Dev Biol.* 2018;80:50–64. doi:10.1016/j.semcdb.2017.05.023
12. Cui Q, Wang JQ, Assaraf YG, et al. Modulating ROS to overcome multi-drug resistance in cancer. *Drug Resist Updat.* 2018;41:1–25. doi:10.1016/j.drug.2018.11.001
13. Slika H, Mansour H, Wehbe N, et al. Therapeutic potential of flavonoids in cancer: ROS-mediated mechanisms. *Biomed Pharmacother.* 2022;146:112442. doi:10.1016/j.biopha.2021.112442
14. Flores-Lopez G, Moreno-Lorenzana D, Ayala-Sanchez M, et al. Parthenolide and DMAPT induce cell death in primitive CML cells through reactive oxygen species. *J Cell Mol Med.* 2018;22(10):4899–4912. doi:10.1111/jcmm.13755
15. Zhu J, Tang C, Cong Z, et al. ACT001 reverses resistance of prolactinomas via AMPK-mediated EGR1 and mTOR pathways. *Endocr Relat Cancer.* 2022;29(2):33–46. doi:10.1530/ERC-21-0215
16. Liu N, Li Y, Chen G, Ge K. Evodiamine induces reactive oxygen species-dependent apoptosis and necroptosis in human melanoma A-375 cells. *Oncol Lett.* 2020;20(4):121. doi:10.3892/ol.2020.11983
17. Hou Y, Sun B, Liu W, et al. Targeting of glioma stem-like cells with a parthenolide derivative ACT001 through inhibition of AEBP1/PI3K/AKT signaling. *Theranostics.* 2021;11(2):555–566. doi:10.7150/thno.49250
18. Sufian HB, Santos JM, Khan ZS, et al. Parthenolide reverses the epithelial to mesenchymal transition process in breast cancer by targeting TGFbeta1: In vitro and in silico studies. *Life Sci.* 2022;301:120610. doi:10.1016/j.lfs.2022.120610
19. Liu D, Han Y, Liu L, et al. Parthenolide inhibits the tumor characteristics of renal cell carcinoma. *Int J Oncol.* 2020;58(1):100–110. doi:10.3892/ijo.2020.5148
20. Liu X, Wang C, Li S, et al. Parthenolide derivatives as PKM2 activators showing potential in colorectal cancer. *J Med Chem.* 2021;64(23):17304–17325. doi:10.1021/acs.jmedchem.1c01380
21. Kouhpaykar H, Sadeghian MH, Rafatpanah H, et al. Synergy between parthenolide and arsenic trioxide in adult T-cell leukemia/lymphoma cells in vitro. *Iran J Basic Med Sci.* 2020;23(5):616–622. doi:10.22038/ijbms.2020.40650.9610
22. Jorge J, Neves J, Alves R, Gerales C, Gonçalves AC, Sarmiento-Ribeiro AB. Parthenolide induces ROS-mediated apoptosis in lymphoid malignancies. *Int J Mol Sci.* 2023;24(11):9167. doi:10.3390/ijms24119167
23. Malumbres M, Barbacid M. Cell cycle, CDKs and cancer: A changing paradigm. *Nat Rev Cancer.* 2009;9(3):153–166. doi:10.1038/nrc2602
24. Ding Y, Chen X, Liu C, et al. Identification of a small molecule as inducer of ferroptosis and apoptosis through ubiquitination of GPX4 in triple negative breast cancer cells. *J Hematol Oncol.* 2021;14(1):19. doi:10.1186/s13045-020-01016-8
25. Karam L, Abou Staiteieh S, Chaaban R, et al. Anticancer activities of parthenolide in primary effusion lymphoma preclinical models. *Mol Carcinog.* 2021;60(8):567–581. doi:10.1002/mc.23324
26. Delbridge ARD, Grabow S, Strasser A, Vaux DL. Thirty years of BCL-2: Translating cell death discoveries into novel cancer therapies. *Nat Rev Cancer.* 2016;16(2):99–109. doi:10.1038/nrc.2015.17
27. Czabotar PE, Lessene G, Strasser A, Adams JM. Control of apoptosis by the BCL-2 protein family: Implications for physiology and therapy. *Nat Rev Mol Cell Biol.* 2014;15(1):49–63. doi:10.1038/nrm3722
28. Park EJ, Chauhan AK, Min KJ, Park DC, Kwon TK. Thymoquinone induces apoptosis through downregulation of c-FLIP and Bcl-2 in renal carcinoma Caki cells. *Oncol Rep.* 2016;36(4):2261–2267. doi:10.3892/or.2016.5019
29. Fatokun AA, Dawson VL, Dawson TM. Parthanatos: Mitochondrial-linked mechanisms and therapeutic opportunities. *Br J Pharmacol.* 2014;171(8):2000–2016. doi:10.1111/bph.12416
30. Yang Y, Chen Y, Wu JH, et al. Targeting regulated cell death with plant natural compounds for cancer therapy: A revisited review of apoptosis, autophagy-dependent cell death, and necroptosis. *Phytother Res.* 2023;37(4):1488–1525. doi:10.1002/ptr.7738
31. Holmgren C, Sunström Thörnberg E, Granqvist V, Larsson C. Induction of breast cancer cell apoptosis by TRAIL and Smac mimetics: Involvement of RIP1 and cFLIP. *Curr Issues Mol Biol.* 2022;44(10):4803–4821. doi:10.3390/cimb44100327
32. Galluzzi L, Bravo-San Pedro JM, Vitale I, et al. Essential versus accessory aspects of cell death: Recommendations of the NCCD 2015. *Cell Death Differ.* 2015;22(1):58–73. doi:10.1038/cdd.2014.137
33. Huang Z, Xia H, Cui Y, Yam JWP, Xu Y. Ferroptosis: From basic research to clinical therapeutics in hepatocellular carcinoma. *J Clin Transl Hepatol.* 2022;11(1):207–218. doi:10.14218/JCTH.2022.00255
34. Scimeca M, Rovella V, Palumbo V, et al. Programmed cell death pathways in cholangiocarcinoma: Opportunities for targeted therapy. *Cancers.* 2023;15(14):3638. doi:10.3390/cancers15143638
35. Steinhart L, Belz K, Fulda S. Smac mimetic and demethylating agents synergistically trigger cell death in acute myeloid leukemia cells and overcome apoptosis resistance by inducing necroptosis. *Cell Death Dis.* 2013;4(9):e802. doi:10.1038/cddis.2013.320